Proc. Natl. Acad. Sci. USA
Vol. 90, pp. 9547–9551, October 1993
Biophysics

Simulation of the kinetics of ligand binding to a protein by molecular dynamics: Geminate rebinding of nitric oxide to myoglobin

(picosecond kinetics/chemical dynamics/lasers)

OLIVIER SCHAAD, HUAN-XIANG ZHOU, ATTILA SZABO, WILLIAM A. EATON, AND ERIC R. HENRY

Laboratory of Chemical Physics, National Institute of Diabetes and Digestive and Kidney Diseases, National Institutes of Health, Bethesda, MD 20892

Communicated by Robert Zwanzig, July 6, 1993 (received for review May 10, 1993)

ABSTRACT **We have begun to use molecular dynamics to simulate the kinetics of nitric oxide rebinding to myoglobin after photodissociation. Rebinding was simulated using a potential function that switches smoothly between a nonbinding potential and a binding potential as a function of the position and orientation of the ligand, with no barrier arising from the crossing of potential surfaces of different electron spin. In 96 of 100 trajectories, the ligand rebound in <15 ps. The kinetic progress curve was obtained by determining the time in each trajectory at which the ligand rebound and then calculating the fraction of unbound ligands as a function of time. The curve can be well reproduced by a simple model based on the dynamics of a Langevin particle moving on a one-dimensional potential of mean force calculated from nonreactive protein trajectories. The rate of escape from the energy well adjacent to the heme is in good agreement with the value calculated from experimental data, suggesting that a multiple-well model provides a plausible explanation for the nonexponential rebinding kinetics. A transition-state analysis suggests that protein conformational relaxation coupled to the displacement of the iron from the heme plane is an unlikely cause for the nonexponential rebinding of nitric oxide.**

Advances in computer technology now make it possible to simulate the kinetics of ultrafast chemical reactions in solution by using the technique of molecular dynamics. One of the fastest known biochemical reactions is the geminate rebinding of nitric oxide to the hemes of hemoglobin and myoglobin. This reaction occurs on a tens of picoseconds time scale and was discovered by Hochstrasser and coworkers (1), after the introduction of picosecond laser technology to the study of proteins in the late 1970s (2). It is the very high speed of this reaction that makes it suitable for calculating the many trajectories that are necessary to obtain statistically meaningful kinetics. The attractive feature of simulating kinetics by classical molecular dynamics is that in principle a complete description of the process (apart from quantum effects) is contained in trajectories run on an accurate potential surface. It should therefore be possible to address important issues and gain insights into the chemical dynamics of ligand binding to myoglobin.

Molecular dynamics simulations of ultrafast laser photolysis experiments began with the work of Henry *et al.* (3). This study showed that the displacement of the iron to near its equilibrium position in deoxyhemoglobin was complete in <200 fs, supporting the interpretation of optical experiments (4). Longer trajectories have shown an additional slower displacement of the iron from the heme plane attributed to conformational relaxation of the protein (5, 6). Other simulations have focused on ligand motion in the protein (7–11).

The publication costs of this article were defrayed in part by page charge payment. This article must therefore be hereby marked "*advertisement*" in accordance with 18 U.S.C. §1734 solely to indicate this fact.

In this study we have simulated photodissociation and geminate rebinding of nitric oxide to myoglobin. The potential surface for rebinding is complex, because the change in spin from a quintet iron and doublet ligand to a doublet iron–ligand complex necessarily introduces an "electronic" barrier arising from the crossing of potential surfaces. Since nothing is known about these surfaces from quantum mechanical calculations, we have for simplicity ignored the electronic barrier and have used a Morse potential for the rebinding surface. This has the effect of artificially speeding up the reaction. Elber and coworkers (12) have independently carried out similar simulations in which an electronic barrier has been included.

METHODS

Molecular dynamics simulations using the program CHARMM23 (13) were performed on the system consisting of the complete myoglobin molecule (Brookhaven Protein Data Bank File 1MBO), including all hydrogen atoms, surrounded by 351 water molecules (14), plus nitric oxide. To simulate the dissociation of ligands and subsequent rebinding, three distinct potential functions for the heme group were employed at different stages of the simulations. These potential functions differ only in the description of interactions involving the set of eight atoms that includes the iron (Fe), the four pyrrole nitrogens (N_p), the nitrogen $N_{\varepsilon 2}$ of the proximal histidine bonded to the iron, and the nitrogen (N) and oxygen (O) of the ligand. The general form of the potential function for these atoms is

$$\begin{aligned} V = {} & D\{1-[1-e^{-\beta(r-r_o)}]^2\} \\ & + s(r)K_\theta(\theta-\theta_o)^2 + s(r)K_\phi(\phi-\phi_o)^2 && \text{[term 1]} \\ & + \sum_{(\mathrm{Fe-N_p})} K_{\mathrm{bp}}(b_p-b_{po})^2 + K_{b\varepsilon}(b_\varepsilon-b_{\varepsilon o})^2 \\ & + \sum_{(\mathrm{N_p-Fe-N_p})} K_{\alpha pp}(\alpha_{pp}-\alpha_{ppo})^2 \\ & + \sum_{(\mathrm{N_p-Fe-N_\varepsilon})} K_{\alpha p\varepsilon}(\alpha_{p\varepsilon}-\alpha_{p\varepsilon o})^2 && \text{[term 2]} \\ & + [1-S(r,\theta,\phi)] \sum_{(\mathrm{N-N_p})} \varepsilon\left[\left(\frac{\sigma}{r}\right)^{12}-\left(\frac{\sigma}{r}\right)^{6}\right] && \text{[term 3]} \end{aligned} \qquad [1]$$

where r is the distance between the iron and the ligand nitrogen (N), θ is the angle Fe–N–O, and ϕ is the angle $N_{\varepsilon 2}$–Fe–N.

The potential function for the liganded heme (6-coordinated iron) was used prior to dissociation. This potential includes iron–ligand bonding interaction terms [labeled term 1 in Eq. 1 with $s(r) = 1$], the first of which is a Morse potential involving the distance between the iron and the

ligand nitrogen. The Morse parameters [r_o = 1.74 Å, D = 23 kcal/mol (1 cal = 4.184 J), and β = 2.7 Å^{-1}] were estimated from x-ray crystallographic, thermodynamic, and vibrational spectroscopic data, respectively (15, 16). The liganded potential also includes terms (labeled term 2) for the rest of the bonding interactions in the iron coordination sphere (specifically the Fe–N_p and Fe–$N_{\varepsilon 2}$ bonds and the N_p–Fe–N_p and N_p–Fe–$N_{\varepsilon 2}$ angles). The force constants (various K values) and equilibrium bond lengths (b_{po} and $b_{\varepsilon o}$) and angles (α_{ppo} and $\alpha_{p\varepsilon o}$) were chosen to produce an essentially planar heme with the iron lying in the plane.

In the unliganded potential the bonding interactions (term 1) between the ligand and heme were replaced by nonbonded interactions between the ligand and the pyrrole nitrogens [terms labeled term 3 with $S(r,\theta,\phi) = 0$], and the parameters for the remaining interactions (term 2) involving the iron were changed to produce a domed heme with the iron ≈0.4 Å out of the plane of the four pyrrole nitrogens (3).

The third potential function, the so-called rebinding potential, was used to describe the heme–ligand system after dissociation was complete. In this function the bonding interactions (term 1) were restored. The switching function $s(r)$ serves to attenuate the angle-bending interactions as the Fe–N distance increases and has the form: $s(r) = 1$ for $r < r_o$ and $s(r) = 1 - \{1 - \exp[-\beta(r - r_o)]\}^2$ for $r > r_o$. The force constants and equilibrium bond lengths and angles for the interactions in term 2 are smoothly switched in the rebinding potential as a function of the ligand position between their liganded and unliganded values. That is, each of these parameters x is given by $x = x_{\text{unliganded}} + S(r,\theta,\phi)\,(x_{\text{liganded}} - x_{\text{unliganded}})$. The switching function $S(r,\theta,\phi)$, which was also used to attenuate the van der Waals interactions (term 3) between the ligand nitrogen and the heme pyrrole nitrogens, is given by: $S(r,\theta,\phi) = 0.25[1 + \tanh\{-W[r - (r_o + \delta)]\}] \times \{[1 + K(\theta - \theta_o)^2]^{-1} + [1 + K(\phi - \phi_o)^2]^{-1}\}$, with W = 6.3 Å^{-1}, δ = 0.7 Å, and K = 3 rad^{-2}. This switching function was designed so that the rebinding potential approximated the unliganded potential when the ligand was far from the iron or at an unfavorable orientation for bond formation and matched the liganded potential when the iron–ligand geometry (r, θ, and ϕ) was optimal for bond formation. Representative potential energy curves for these potentials are shown in Fig. 1.

The photodissociation event was simulated by instantaneously changing the potential function of the heme–ligand system from the liganded potential to the unliganded potential. This replaces the bonding interactions between the ligand and the heme with nonbonded interactions between the ligand and the pyrrole nitrogens, which propel the ligand away from the heme. The rebinding event was simulated by changing from the unliganded potential to the rebinding potential, either when the energy calculated using the unliganded potential becomes less than that calculated using the rebinding potential or when r first exceeds 4.0 Å and no repulsive interactions remain between the ligand and the pyrrole nitrogens.

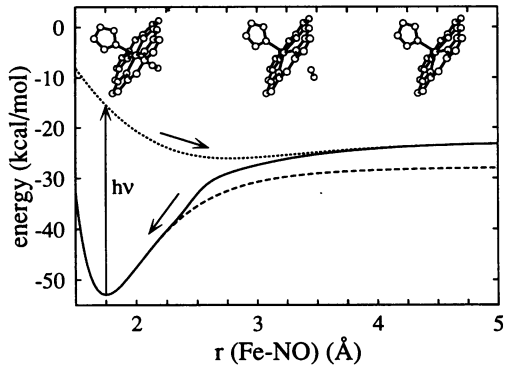

FIG. 1. Energy of the histidine–heme–NO system as a function of the Fe–N distance for the liganded (dashed curve), unliganded (dotted curve), and rebinding (unbroken curve) potentials. Each curve was obtained by minimizing the energy using the appropriate potential function, with the Fe–NO distance being constrained at a fixed distance along the heme normal. All of the parameters were the same as those given by Henry *et al.* (3) except for K_θ = 35 kcal per mol per rad^2, θ_o = 140°, and K_ϕ = 45 kcal per mol per rad^2.

RESULTS AND DISCUSSION

Kinetic Progress Curves for Ligand Rebinding. The simplest property of the photodissociation/recombination trajectories to monitor is the distance between the heme iron and the nitrogen of the nitric oxide ligand. Fig. 2*A* shows iron–ligand distances as a function of time from a set of 20 trajectories. All of the trajectories originated from the same 200-ps liganded trajectory and were started by initiating dissociation at 5-ps intervals from the last 100 ps of the trajectory. In <0.1

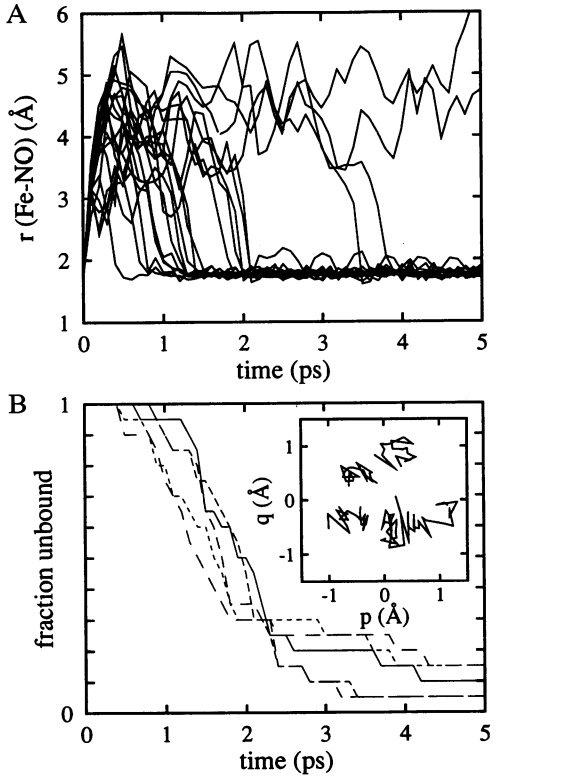

FIG. 2. Trajectories and kinetics of ligand rebinding. Five liganded trajectories were produced by using different seeds for the random number generator used in heating the system. (*A*) Fe–NO distances as a function of time for each of the 20 photodissociation events produced from a single liganded trajectory. (*B*) Kinetics of ligand rebinding. Each line represents, for the set of 20 dissociation simulations produced from a single liganded trajectory, the fraction of unrebound ligands as a function of time. (*Inset*) Approximate two-dimensional representation of the overall conformation of the molecule in each of the 100 dissociation simulations. Structures were produced by energy minimizing the coordinates of the system at each dissociation event and least-squares superimposing the resulting 100 coordinate sets onto a fixed coordinate set to remove effects of net rotations and translations of the molecule within and among the trajectories. An approximate two-dimensional representation of the complete set of structures was produced using a least-squares projection method (17, 18). Shown are the 100 pairs (p_i,q_i) that optimally reproduce the "true" distance matrix, with a mean error of 0.22 Å. Conformations produced from the same baseline simulation are connected by lines.

ps, the ligand moves to a position >3 Å from the iron, and in all but 2 trajectories rebinds within 5 ps. Twenty trajectories are clearly insufficient for a kinetic description. To explore the possible role of different protein conformations, we calculated 4 additional sets of 20 trajectories, each set originating from a different 200-ps liganded trajectory. To classify the conformation associated with each dissociation trajectory, the structure at each dissociation event was energy-minimized. An approximate two-dimensional representation (17, 18) of the resulting 100 structures is shown in Fig. 2 *Inset*. Each liganded trajectory produces structures in a distinct region of this two-dimensional conformational space, which may be thought of loosely as representing a distinct "conformational substate."

Fig. 2*B* shows the kinetic progress curves calculated from the rebinding times in the five sets of 20 trajectories. The kinetic progress curve for each set, or conformational substate, is calculated as the fraction of ligands that remain unbound as a function of time. There is very little difference among the progress curves for the five substates. All exhibit a lag phase before ligand rebinding begins, varying from 0.4 ps to 0.8 ps, followed by a roughly exponential decay. This lag phase arises from the fact that the ligand is initially moving away from the iron. For the 11 trajectories in which rebinding did not occur by 5 ps, the simulation was continued for an additional 10 ps. Rebinding occurred in 7 of these 11 trajectories. Thus, in all but 4 of the 100 trajectories, ligand rebinding occurred within 15 ps. Since escape is a rare event, we estimate using the standard deviation of a Poisson process that the uncertainty in this number is ±2 (i.e., the square root of the mean).

Fig. 3 shows the positions of the ligand within the protein as a function of time. In all trajectories in which the ligand rebinds within 15 ps, it remains in a pocket very close to the iron. This pocket is formed by the heme and side chains from five protein residues. The frequencies of collisions of the dissociated ligand with these residues are in the order Val-68 > Phe-43 > Ile-107 > Leu-29 > His-64. In the four trajectories in which the rebinding did not occur within 15 ps, the ligand had escaped from this pocket. The picture that emerges from the simulations, then, is that upon dissociation there is a competition between very fast geminate rebinding and escape from a heme pocket.

Fig. 4 shows the kinetic progress curve calculated from all 100 trajectories. After the lag phase, the decay is roughly exponential, so that three parameters are sufficient to describe this curve—the length of the lag phase = 0.4 ps, the time constant for rebinding = 2 ps, and the fraction that rebind within 15 ps (the geminate yield) = 0.96. The experimentally determined rebinding curve (5) is rather different. The experimental curve was well described by several different functions, including a double exponential with time constants of 28 ps and 280 ps and almost equal amplitudes (5) (there was no report of a lag phase in the data, but it is not clear whether a 0.4-ps lag could have been detected). This difference is expected because of the absence of an electronic barrier in the simulations.* Nevertheless, our simulations immediately suggest a simple interpretation of the experimental results, namely, that the 28-ps relaxation corresponds to binding from the heme pocket and that the multiexponential nature of the rebinding is a reflection of the existence of multiple wells inside the protein.

Our simulations are consistent with the kinetic scheme:

*It is interesting to note that Petrich *et al.* (19) found a 2.5-ps relaxation in hemoglobin, myoglobin, and protoheme which they interpreted as arising from the barrierless rebinding of ligands (NO, O_2, and CO) to an excited singlet state of the deoxyheme, which is also observed in the simulations of Elber and coworkers (12).

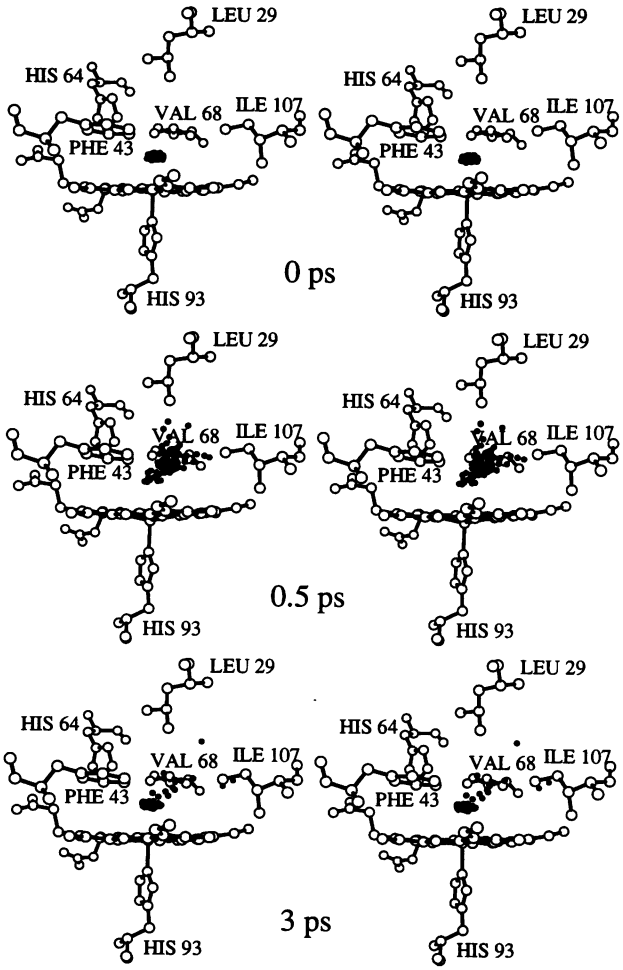

FIG. 3. Distribution of ligand positions before photodissociation and at 0.5 ps and 3 ps after photodissociation. The position of the ligand at the specified time after dissociation in each of the 100 dissociation simulations is shown, as well as the instantaneous structures at the same time points of the heme, proximal histidine, and five side chains that form the pocket for the ligand (see text), averaged over the 100 simulations.

$$\mathrm{MbNO} \underset{k_b}{\overset{h\nu}{\rightleftarrows}} \mathrm{Mb{\cdot}NO} \overset{k_e}{\rightleftarrows} \mathrm{Mb{\cdot}\cdot\cdot NO}, \qquad [2]$$

where Mb·NO represents the geminate state with the ligand in the heme pocket and Mb· · ·NO is the geminate state with the ligand in one or more outer protein wells. In this scheme the relaxation rate $k = k_b + k_e$ and the geminate yield $\phi = k_b/(k_b + k_e)$. The inverse escape rate, $1/k_e$, can be calculated from the simulated geminate yield ($\phi = 0.96 \pm 0.02$) and the simulated relaxation rate [$k = 0.6 \pm 0.03$; $k_e = k(1 - \phi)$] to be 40 ± 20 ps. A corresponding calculation using the experimental results for the first relaxation of the biexponential fit ($1/k = 28 \pm 3$ ps and $\phi = 0.52 \pm 0.05$) gives 58 ± 12 ps. The agreement between the escape rates calculated from the simulations and experiments lends support to the notion that the biexponential behavior of the experimental rebinding curve could arise from rebinding from inner and outer wells in the protein (Eq. 2).

Using the above model we can estimate the contribution to the geminate rebinding rate from the electronic barrier by comparing the simulated and experimental $k_b = k - k_e$. From the simulations $1/k_b = 1.6$ ps, while the experimental $1/k_b = 53$ ps. There are two sources to this 33-fold slowing of the rate by the electronic barrier. One is the barrier height, and the second is the probability that the net spin of the system will

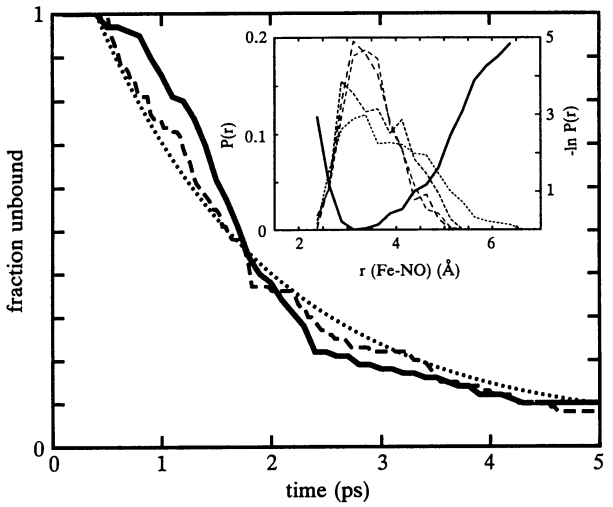

FIG. 4. Simulated kinetics of rebinding. The solid curve is the result from 100 trajectories (the average of the five curves in Fig. 2*B*). The dotted curve is a fit using a single exponential decay with a delayed onset. The dashed curve is the result of 100 Langevin simulations run on the potential of mean force. (*Inset*) Distribution of ligand positions in four nonreactive trajectories (broken curves) and potential of mean force (unbroken curve), $U(r)/k_BT = -\ln P(r)$.

not change, in which case the iron–ligand system will not remain on the adiabatic surface (12, 20).

A Simple Model of Ligand Rebinding: Langevin Dynamics on a Potential of Mean Force. In addition to an electronic barrier from potential surface crossing, there are two additional contributions to the free energy barrier to ligand rebinding. One of these is steric interference from distal residues, and the other is the requirement that the ligand becomes localized close to the iron with the correct orientation. The latter effect produces a pure entropic barrier, while the former can produce both energetic and entropic contributions. To assess the magnitude of these effects and to provide further evidence for a pocket very close to the iron atom, six nonreactive 50-ps trajectories were run on the unliganded potential surface. In four of these, the ligand was trapped for the entire length of the trajectory in the same well from which rebinding occurs in the reactive trajectories. The potential of mean force for the iron–ligand distance, $U(r)$, that describes this well was calculated from the four trajectories by counting the number of configurations with a given iron–ligand distance, r, and is shown in Fig. 4 *Inset*.

To construct a simple dynamical picture consistent with the simulated kinetic progress curves, we modeled the motion along r by the Langevin equation: $M\dot{v} = -\partial U(r)/\partial r - \gamma M v + R(t)$, where $v = dr/dt$ and $R(t)$ is a random force. An effective mass of 10.6 atomic mass units was found using $M = k_BT/\langle v^2\rangle$, where the average was calculated from the nonreactive trajectories. With a collision frequency $\gamma = 10$ ps^{-1}, both the position and velocity autocorrelation functions were reasonably well reproduced. The motion of the ligand in the heme pocket is not diffusive but somewhat underdamped, as the effective harmonic frequency of the well is $\omega = [k_BT/M(\langle r^2\rangle - \langle r\rangle^2)]^{1/2} = 11$ ps^{-1} and critical damping occurs when $\gamma/2 = \omega$. The formation of the heme–NO complex was modeled by placing an absorbing wall at $r = r^{\ddagger}$. Photodissociation was implicitly modeled using the iron–ligand distance and the corresponding velocity at 0.4 ps obtained from reactive molecular dynamics as the initial conditions of the Langevin particle. (Of course, 0.4 ps had to be added to the survival time.) Fig. 4 compares the kinetic progress curves from the Langevin and protein simulations for $r^{\ddagger} = 2.7$ Å. (This distance was varied to obtain best agreement.) The free energy at $r^{\ddagger} = 2.7$ Å is only 0.7 k_BT above the minimum in the potential of mean force and may be regarded as a rough estimate of the magnitude of the barrier due to steric interference and entropic effects described at the beginning of this section. The small magnitude of this barrier supports the notion that the bent Fe–N–O geometry allows the ligand to bind to the heme without significant steric barriers (21).

Nonexponential Rebinding, Protein Relaxation, and the Structure of the Transition State. Another possible cause of nonexponential geminate rebinding of NO is a time-dependent change in the rebinding rate due to conformational relaxation. Anfinrud and coworkers (22) have found a time-dependent shift in the frequency of a charge-transfer band (23) after photodissociation of MbCO that can be attributed to conformational relaxation of the protein (24) that begins at less than a few picoseconds and persists to nanoseconds. One detailed interpretation of this frequency change is that it reflects the motion of the iron out of the heme plane (23, 25) after its initial (<200 fs) displacement (3–6). Simulations by Kuczera *et al.* (6) show a time-dependent shift in the iron position that in fact superimposes on the frequency shift. They observe changes of >0.1 Å between 1 and 100 ps. No such changes are observed in our simulations (Fig. 5) or those of Li *et al.* (12). One possible explanation for the difference in the simulation results is that Kuczera *et al.* (6) used a heme potential that resulted in an out-of-(porphyrin) plane displacement that was already larger at 100 ps (0.60 Å) than the known equilibrium value from x-ray crystallography of 0.55 Å (26), thereby producing a protein response.

In any event, the experiments of Anfinrud and coworkers (22) demonstrate that some kind of protein relaxation is occurring. Is this relaxation relevant to NO rebinding? In the case of the *R* and *T* conformations of hemoglobin, the overall bimolecular rates for NO rebinding are the same (21, 27). Murray *et al.* (28) have shown that the rates for CO motion within the protein are most probably the same for the two conformations, so that comparing bimolecular rates for diatomic ligands is equivalent to comparing binding rates at the heme. Szabo (21) pointed out that the results for the NO rates could be explained by postulating a transition state in which the iron is still in its out-of-plane deoxy conformation. If the iron does not move in passing from the reactant state to the transition state, the protein conformation that is controlling the iron displacement would have no influence on the binding rate. This analysis does not support the suggestion (5, 6) that protein relaxation coupled to the displacement of the iron from the heme plane is responsible for the nonexponential rebinding of NO. It also suggests that there is no contribution to the nonexponential rebinding of NO from conformational substates with different iron displacements that do not interconvert rapidly on the time scale of NO rebinding. Conformational relaxation could, however, contribute to the non-

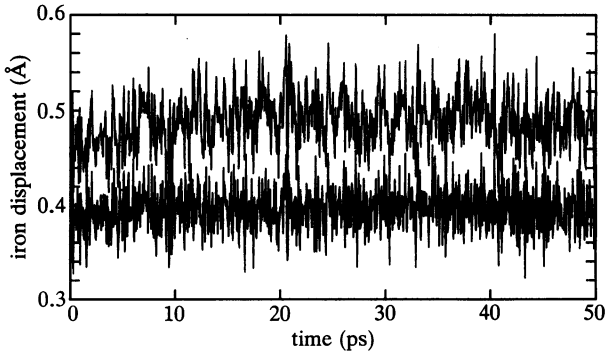

FIG. 5. Displacement of iron from plane of pyrrole nitrogens (lower curve) and plane of 24 porphyrin skeletal atoms (upper curve) in nonrebinding trajectories. The curves are the averages of the displacements from 12 trajectories.

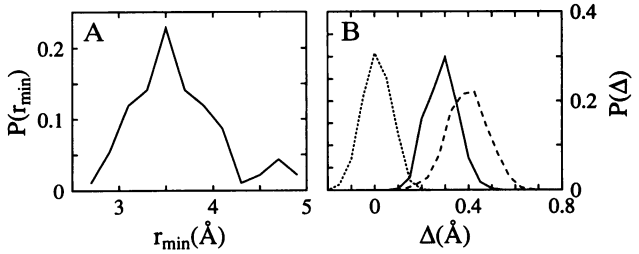

FIG. 6. Analysis of the iron displacement in the transition state for ligand rebinding. (*A*) The distribution of values of r_{min} from 100 trajectories. For each dissociation trajectory, the quantity r_{min} is defined as the closest distance the ligand can approach the iron without rebinding. The smallest such distance is 2.7 Å. (*B*) The distribution of iron out-of-pyrrole plane displacements: liganded molecule (dotted curve), unliganded molecule (dashed curve), and molecule in the classical transition state (solid curve)—i.e., at an iron–ligand distance of 2.7 Å on the path to rebinding.

exponential rebinding of CO, where the iron is believed to be closer to the heme plane in the transition state and where protein relaxation and geminate rebinding occur simultaneously on a nanosecond time scale (29–31).

This discussion raises the question of the heme conformation in the transition state predicted by the simulations. We can address this question in the following way. Fig. 6*A* shows that the smallest iron–ligand distance without immediate rebinding is 2.7 Å. That is, all ligands that come closer to the iron than 2.7 Å will proceed on to binding. This distance may be regarded as the position of the dividing surface of classical transition state theory (interestingly, the same distance that was required in the Langevin model for rebinding). Fig. 6*B* shows the distribution of iron displacements at 2.7 Å in the rebinding trajectories. As expected for the barrierless rebinding considered here, the iron displacement is much closer to that of deoxymyoglobin than to that of the liganded complex. Since trajectories can recross the dividing surface at the true classical transition state, 2.7 Å must be considered the minimum iron–ligand distance in the transition state for these simulations, and, correspondingly, the distribution of iron displacements should be considered the least deoxy-like. The finding of a deoxy-like transition state in the simulations is consistent with the lack of any observable effect on the influence of conformational substates on the rebinding rates (Fig. 2*B*).

In conclusion we should point out that the present work should be regarded as only a first step in simulating ligand binding to heme proteins by molecular dynamics. At this point both experimental data and theoretical input from quantum mechanical calculations are very much needed to give an accurate description of the dissociative and rebinding potential surfaces. This information will be necessary to perform more realistic simulations.

We thank Bernard R. Brooks and Milan Hodoscek for much help in the use of the program CHARMM, and the Division of Computer Research and Technology of the National Institutes of Health for use of their Intel computer. We also thank Philip Anfinrud, Ron Elber, and Martin Karplus for sending us preprints of their work. O.S. thanks the Swiss National Science Foundation for a fellowship.

1. Cornelius, P. A., Hochstrasser, R. M. & Steele, A. W. (1983) *J. Mol. Biol.* **163,** 119–128.
2. Greene, B. I., Weisman, R. B., Hochstrasser, R. M. & Eaton, W. A. (1978) *Proc. Natl. Acad. Sci. USA* **75,** 5255–5259.
3. Henry, E. R., Levitt, M. & Eaton, W. A. (1985) *Proc. Natl. Acad. Sci. USA* **82,** 2034–2038.
4. Martin, J. L., Migus, A., Poyart, C., Lecarpentier, Y., Astier, R. & Antonetti, A. (1983) *Proc. Natl. Acad. Sci. USA* **80,** 173–177.
5. Petrich, J. W., Lambry, J. C., Kuczera, K., Karplus, M., Poyart, C. & Martin, J. L. (1991) *Biochemistry* **30,** 3975–3987.
6. Kuczera, K., Lambry, J. C., Martin, J. L. & Karplus, M. (1993) *Proc. Natl. Acad. Sci. USA* **90,** 5805–5807.
7. Kottalam, J. & Case, D. A. (1988) *J. Am. Chem. Soc.* **110,** 7690–7697.
8. Elber, R. & Karplus, M. (1990) *J. Am. Chem. Soc.* **112,** 9161–9175.
9. Straub, J. E. & Karplus, M. (1991) *Chem. Phys.* **158,** 221–248.
10. Gibson, Q. H., Regan, R., Elber, R., Olson, J. S. & Carver, T. E. (1992) *J. Biol. Chem.* **267,** 22022–22034.
11. Case, D. A. & Karplus, M. (1979) *J. Mol. Biol.* **132,** 343–368.
12. Li, H., Elber, R. & Straub, J. E. (1993) *J. Biol. Chem.* **268,** 17908–17916.
13. Brooks, B. R., Bruccoleri, R. E., Olafson, B. D., States, D. J., Swaminathan, S. & Karplus, M. (1983) *J. Comp. Chem.* **4,** 187–217.
14. Steinbach, P. J., Loncharich, R. J. & Brooks, B. R. (1991) *Chem. Phys.* **158,** 383–394.
15. Barisas, B. G. (1986) in *Thermodynamic Data for Biochemistry and Biotechnology*, ed. Hinz, H.-J. (Springer, New York), pp. 234–255.
16. Scheidt, W. R., Brinegar, A. C., Ferro, E. B. & Kirner, J. F. (1977) *J. Am. Chem. Soc.* **99,** 7315–7322.
17. Levitt, M. (1983) *J. Mol. Biol.* **168,** 621–657.
18. Henry, E. R. (1993) *Biophys. J.* **64,** 869–885.
19. Petrich, J. W., Poyart, C. & Martin, J. L. (1988) *Biochemistry* **27,** 4049–4060.
20. Frauenfelder, H. & Wolynes, P. G. (1985) *Science* **229,** 337–345.
21. Szabo, A. (1978) *Proc. Natl. Acad. Sci. USA* **75,** 2108–2111.
22. Lim, M., Jackson, T. A. & Anfinrud, P. A. (1993) *Proc. Natl. Acad. Sci. USA* **90,** 5801–5804.
23. Eaton, W. A., Hanson, L. K., Stephens, P. J., Sutherland, J. C. & Dunn, J. B. R. (1978) *J. Am. Chem. Soc.* **100,** 4991–5003.
24. Kuriyan, J., Wilz, S., Karplus, M. & Petsko, G. A. (1986) *J. Mol. Biol.* **192,** 133–154.
25. Murray, L. P., Hofrichter, J., Henry, E. R. & Eaton, W. A. (1988) *Biophys. Chem.* **29,** 63–76.
26. Takano, T. (1977) *J. Mol. Biol.* **110,** 569–584.
27. Cassoly, R. & Gibson, Q. H. (1975) *J. Mol. Biol.* **91,** 301–313.
28. Murray, L. P., Hofrichter, J., Henry, E. R., Ikeda-Saito, M., Kitagishi, K., Yonetani, T. & Eaton, W. A. (1988) *Proc. Natl. Acad. Sci. USA* **85,** 2151–2155.
29. Lambright, D. G., Balasubramanian, S. & Boxer, S. G. (1991) *Chem. Phys.* **158,** 249–260.
30. Ansari, A., Jones, C. M., Henry, E. R., Hofrichter, J. & Eaton, W. A. (1992) *Science* **256,** 1796–1798.
31. Tian, W. D., Sage, J. T., Srajer, V. & Champion, P. M. (1992) *Phys. Rev. Lett.* **68,** 408–411.